Hybrid simulation with dynamic substructuring of masonry structures: A numerical study

13TH CANADIAN MASONRY SYMPOSIUM
HALIFAX, CANADA
JUNE 4TH – JUNE 7TH 2017

HYBRID SIMULATION WITH DYNAMIC SUBSTRUCTURING OF MASONRY STRUCTURES: A NUMERICAL STUDY

Abbiati, Giuseppe[1], Miraglia, Gaetano[2], Mojsilović, Nebojša[3], Stojadinović, Božidar[4]

ABSTRACT
Hybrid simulation is used to compute the time history response of an emulated system subject to a dynamic excitation by combining a physical and a numerical substructure. The former is tested in the laboratory by means of servo-controlled actuators whist a real-time computer simulates the latter and solves the coupled equation of motion. Hybrid simulation has been extensively applied for seismic response history analysis of steel and concrete frame structures. For these systems, subdomain partitioning follows storey levels and nodal joints among beam/column-like elements. In the case of planar masonry structures, distributed interfaces characterize system subdomains and, in principle, several actuators should be used to impose the correct boundary conditions to the tested specimen. This paper presents a new substructuring method for planar masonry substructures, which aims to reduce the number of actuators necessary to achieve a predetermined coupling accuracy between physical and numerical subdomains. The numerical validation of this procedure is illustrated for a masonry building facade system.

KEYWORDS: *Seismic analysis; hybrid simulation; dynamic substructuring; non-matching interfaces.*

1 INTRODUCTION

Hybrid Simulation (HS), which is also known as Hardware-in-the-Loop (HiL) testing, has been introduced in the 1970s to simulate the seismic response of civil structures [1,2]. The hybrid model of the emulated system combines numerical and physical subdomains (NS and PS) and its dynamic response to a realistic excitation is simulated using a numerical time-stepping response history analysis. A computer-controlled system applies displacements to the PS using hydraulic/electric servo-actuators and corresponding restoring forces are measured from these degrees of freedom

[1] Post-doctoral Researcher, Institute of Structural Engineering, ETH Zurich, 8093 Zurich., Stefano-Franscini-Platz 5, Switzerland, abbiati@ibk.baug.ethz.ch
[2] PhD student, DAD, Department of Architecture and Design, Polytechnic of Turin, 24 Corso Duca degli Abruzzi, Turin, Italy, getano.miraglia@polito.it
[3] Senior Scientist, Institute of Structural Engineering, ETH Zurich, 8093 Zurich., Stefano-Franscini-Platz 5, Switzerland, mojsilovic@ibk.baug.ethz.ch
[4] Professor, Institute of Structural Engineering, ETH Zurich, 8093 Zurich., Stefano-Franscini-Platz 5, Switzerland, stojadinovic@ibk.baug.ethz.ch

(DOFs) using load cells and fed back to the hybrid model. Then the equation of motion is solved at the next time step. When the response of the PS does not depend on the rate of loading, a pseudodynamic (PSD) HS can be performed at an extended time scale, typically in the broad range of 50-200 times slower than the actual earthquake, requiring inertia and damping forces to be modelled numerically. Real-time (RT) HS is a special case of PSD-HS when a unit time scale is applied. Lack of reliable mathematical models or strongly nonlinear responses justify the experimental substructuring of a system subcomponent, i.e. the PS, while well-known subparts are instantiated in a numerical simulation software, namely computational environment, as NS. HS has been extensively applied for seismic response history analysis of steel and concrete frame structures. However, in the authors' knowledge, there is still a paucity of applications to planar masonry structures. Paquette and Bruneau, [3,4], used PSD-HS to understand the flexible-floor/rigid-unreinforced-wall interaction during earthquake and the effectiveness of the use of fiberglass strips for retrofitting purposes. Pinto and co-workers, [5], performed PSD-HS of different historical constructions subjected to earthquake loading. The extreme sensitivity of friction-based analytic models with respect to assumed friction coefficients motivated Buonopane and White to simulate the seismic response of a frame infilled with masonry by means of PSD-HS, [6]. Along the same line, [7], assessed the seismic performance of a multi-story infilled frame through PSD-HS and observed a strong correlation between wall damage and hysteretic energy dissipation. In all these cases, an entire facade of a masonry building was substructured in the laboratory and treated as a frame with storey masses lumped at the corresponding levels. However, this is not possible, for example, when only a portion of the wall is substructured in the laboratory and distributed boundaries characterize subdomain interfaces. In this case, several actuators should be used to impose the correct boundary condition to the PS, [8,9]. This perspective motivated the authors to develop a new substructuring method for planar masonry structures. The procedure is illustrated for a virtual case study consisting on a simple Planar Masonry Facade System (PMFS) subjected to gravity and seismic loads. A portion of the PMFS is supposed to be substructured in the laboratory as floating PS while the remainder is treated as NS. In common practice, a geometric transformations eliminate rigid body translations and rotations and the only deformational component of the PS displacement response is applied to the tested specimen, which is typically fixed to a loading frame. Accordingly, a Reference (R) Finite Element (FE) partitioned model of the structure is implemented in Matlab, [10], and separated analyses of deformational components of the PS response owing to gravity and seismic loads support the determination of simplified coupling conditions. In order to impose piecewise affine displacement fields along subdomain boundaries and reduce the number of connected nodes, rigid Interface Super-elements (ISs) are introduced on both NS and PS boundaries. In detail, rigid beam and link elements forms the NS interface super-element while steel frames, anchors and connection rods form the PS interface super-element, which imposes simplified interface boundary conditions to the PS in the laboratory. A Modified (M)-FE partitioned model of the PMFS, which incorporates rigid ISs, is used to validate the proposed approach in pure numerical simulation. Finally, a possible experimental

setup is illustrated, which is based on a typical three-actuator setup used for quasi-static cyclic test of masonry walls.

2 DESCRIPTION OF THE CASE STUDY

This section describes the Planar Masonry Facade System (PMFS) as well as the Reference Finite Element (R-FE) partitioned model used to validate the substructuring method.

2.1 Planar masonry facade system

A rectangular shape of 9.6 x 6.6 m size with three openings and a uniform wall thickness of equal to 0.6 m characterizes the geometry of the PMFS, which is reported in Figure 1.

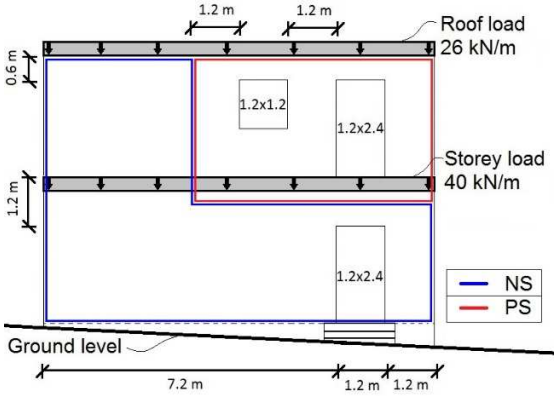

Figure 1: Geometry of the PMFS with static loads and main dimensions

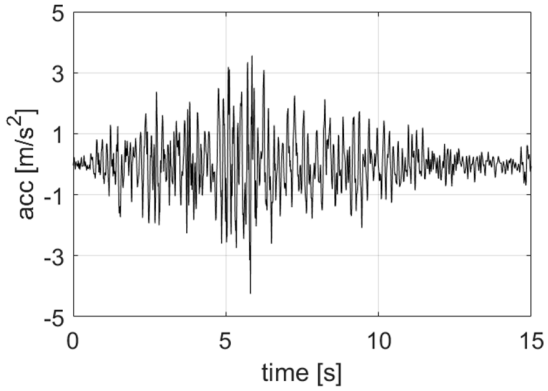

Figure 2: Record of Loma Prieta earthquake, 1989

The PMFS carries gravity loads owing to self-weight and storey masses (equal to 40 kN/m and 26 kN/m for the first and last floor, respectively), and it is subjected to a transversal seismic excitation, which is represented by an accelerogram of the Loma Prieta earthquake of 1989 recorded from the UCSC station; see Figure 2 in this respect. In order to observe the crack pattern in the proximity of the upper openings, a portion of the PMFS is virtually substructured in the laboratory (PS) whilst the remaining portion of the PMFS is simulated in the computer (NS).

2.2 Numerical modeling

In order to simulate the hybrid physical/numerical substructuring of the PMFS a 196-node and 156-element R-FE partitioned model was implemented in the MATLAB environment, [10], according to partitioning scheme of Figure 1. To this end, a linear 4-node membrane element was coded in MATLAB and verified against the ANSYS PLANE element, [11], as reference benchmark. A uniform linear isotropic elastic material was assigned to the entire PMFS, which is characterized by Young elastic modulus E of 0.650 GPa, Poisson ratio υ equal to 0.35 and density ρ of 1900 kg/m^3. Figure 3 shows the R-FE partitioned model of the PMFS with NS and PS partitioning highlighted.

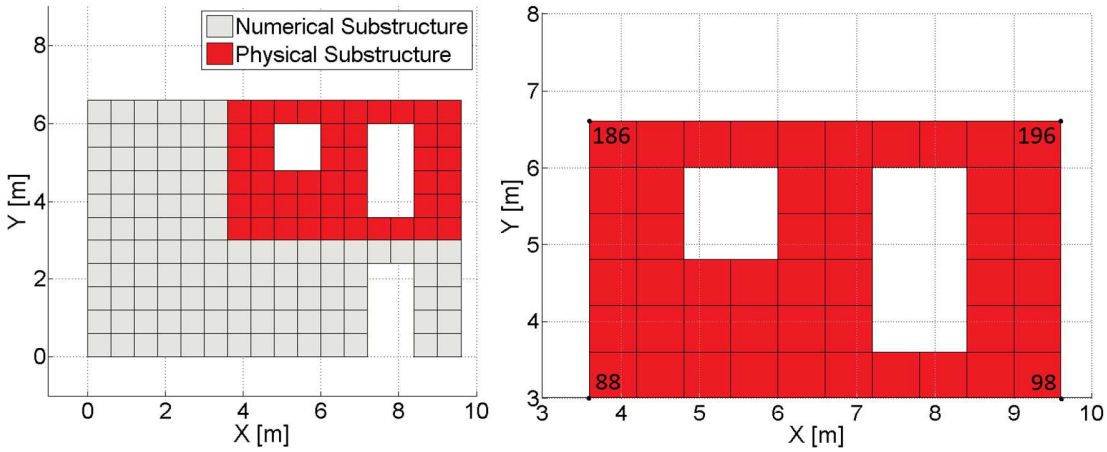

Figure 3: R-FE partitioned model of the PMFS.

For the sake of clarity, a generic system DOF is indicated with the corresponding node number and direction of the displacement component, e.g. 196-X corresponds to the X displacement of node 196. In order to retain all substructure interface DOFs, a dual-assembly procedure based on Localized Lagrange Multipliers (LLM) was used to derived the coupled equations of motion, [12], which read:

$$\begin{cases} \mathbf{M}^N\ddot{\mathbf{u}}^N + \mathbf{C}^N\dot{\mathbf{u}}^N + \mathbf{K}^N\mathbf{u}^N = \mathbf{L}^{N^T}\boldsymbol{\Lambda}^N + \mathbf{F}^N(t) \\ \mathbf{M}^P\ddot{\mathbf{u}}^P + \mathbf{C}^P\dot{\mathbf{u}}^P + \mathbf{K}^P\mathbf{u}^P = \mathbf{L}^{P^T}\boldsymbol{\Lambda}^P + \mathbf{F}^P(t) \end{cases} \tag{1a}$$

$$\begin{cases} \mathbf{L}^N\dot{\mathbf{u}}^N + \bar{\mathbf{L}}^N\dot{\mathbf{u}}_g = \mathbf{0} \\ \mathbf{L}^P\dot{\mathbf{u}}^P + \bar{\mathbf{L}}^P\dot{\mathbf{u}}_g = \mathbf{0} \end{cases} \tag{1b}$$

$$\bar{\mathbf{L}}^{N^T}\boldsymbol{\Lambda}^N + \bar{\mathbf{L}}^{P^T}\boldsymbol{\Lambda}^P = \mathbf{0} \tag{1c}$$

In this specific case, superscripts N and P refer to NS and PS subdomains, respectively. With regard to a generic subdomain l, $\mathbf{M}^{(l)}, \mathbf{C}^{(l)}$ and $\mathbf{K}^{(l)}$ are the mass, the damping and the stiffness matrices while $\ddot{\mathbf{u}}^{(l)}, \dot{\mathbf{u}}^{(l)}$ and $\mathbf{u}^{(l)}$ denote acceleration, velocity and displacement vectors. $\mathbf{L}^{(l)}$ and $\bar{\mathbf{L}}^{(l)}$ are Boolean signed matrices that collocates interface DoFs within the single subdomain and the reference DoF vector, respectively. Vector $\mathbf{F}^{(l)}(t)$ represents the external time-varying load. Lagrange multiplier vectors $\boldsymbol{\Lambda}^{(l)}$ represent interface force fields enforcing kinematic compatibility among subdomains and the reference DoF vector $\mathbf{u}_g$. Figure 4 summarizes the main results of the modal analysis of the R-FE partitioned model.

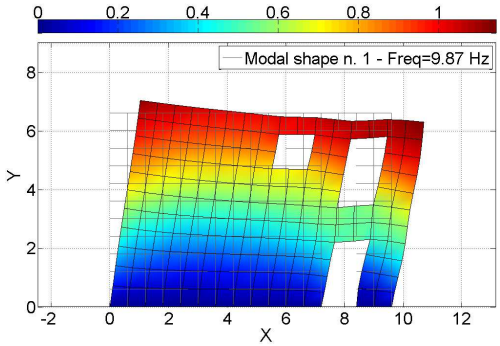

Mode	Frequency (Hz)
1	9.87
2	21.69
3	22.87
4	25.33
5	28.51

Figure 4: Modal analysis of the PMFS.

As shown in Figure 4, Mode #1 is characterized by the global translation of the PMFS along the X direction.

3 SIMPLIFIED COUPLING CONDITIONS

3.1 Deformational response of the physical substructure

In the common practice of HS, a geometric transformation compensates the rigid-body response the PS, which is constrained to a loading frame, and the sole deformational component of the PS response is applied to the tested specimen. Rigid body modes of the PS are defined as,

$$\mathbf{\Phi}^P = ker(\mathbf{K}^P) \tag{2}$$

where $ker(\cdot)$ is the kernel of a generic matrix $(\cdot)$. In order to extract the pure deformational component of the PS response, a number of DOFs equal to the number of rigid body modes is constrained. Figure 5 depicts the constraint setting of the PS.

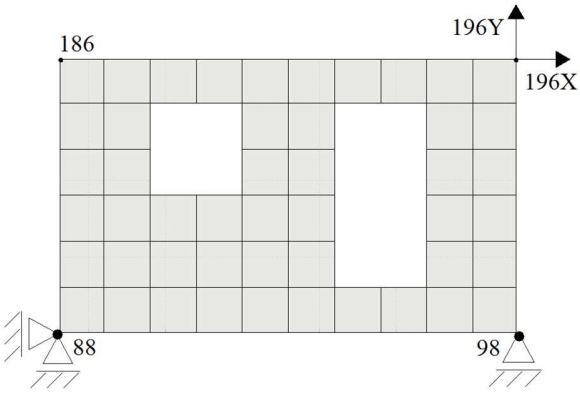

List of constrained DOFs

Node	Direction
88	X
88	Y
89	Y

Figure 5: Constraint setting of the PS.

The pure deformational component of the PS response, which is applied to the tested specimen, reads:

$$\tilde{\mathbf{u}}_k^{P,r} = \mathbf{u}_k^{P,r} + \boldsymbol{\Phi}^{P,r}\boldsymbol{\alpha}_k^P \tag{3}$$

where the rigid body response vector $\boldsymbol{\alpha}_k^P$ is calculated as:

$$\boldsymbol{\alpha}_k^P = -\boldsymbol{\Phi}^{P,c^{-1}}\mathbf{u}_k^{P,c} \tag{4}$$

with

$$\boldsymbol{\Phi}^P = \begin{bmatrix}\boldsymbol{\Phi}^{P,r}\\ \boldsymbol{\Phi}^{P,c}\end{bmatrix}, \mathbf{u}_k^P = \begin{bmatrix}\mathbf{u}_k^{P,r}\\ \mathbf{u}_k^{P,c}\end{bmatrix} \tag{5}$$

where superscripts r and c stand for retained and constrained DOFs whilst subscript k represents a generic time step of the response history.

3.2 Static analysis considering gravity loads

The static analysis of the coupled system response is performed using a version of the algorithm proposed by Farhat and Roux, [13] enhanced to the LLM framework, [12]. Accordingly, loading vectors $\mathbf{F}^N(t)$ and $\mathbf{F}^P(t)$ include gravity loads only.

$$\mathbf{F}^{(l)}(t) = -\mathbf{M}^{(l)}\mathbf{T}_g^{(l)}g \tag{6}$$

where the subscripts indicate a generic subdomain l and $\mathbf{T}_g^{(l)}$ is a Boolean vector defined according to the direction of the gravity acceleration g. Figure 6 depicts the pure deformational component of the displacement response of the PS subjected to gravity loads only.

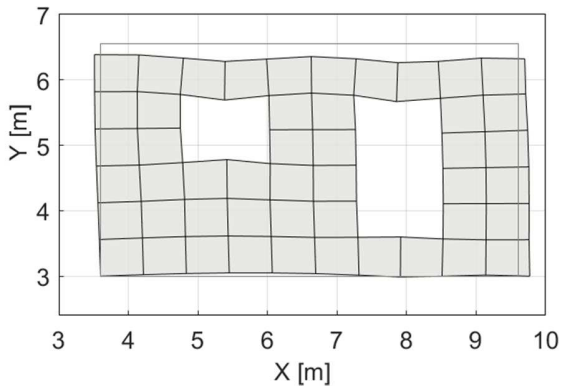

Figure 6: Deformed shape of the PS owing to gravity load.

As shown in Figure 6, the static analysis reveals an almost uniform lowering of wall top.

3.3 Principal component analysis of the seismic response

A version of the time integration algorithm proposed by Gravouil and Combescure, [14] enhanced to LLM framework, [12], was used to simulated the dynamic response of the R-FE partitioned

model defined in Section 2.2 subjected to seismic load. In this case, loading vectors $\mathbf{F}^N(t)$ and $\mathbf{F}^P(t)$ are defined as,

$$\mathbf{F}^{(l)}(t) = -\mathbf{M}^{(l)}\mathbf{T}_{a_g}^{(l)}a_g(t) \tag{7}$$

where the subscripts indicate a generic subdomain l and $\mathbf{T}_{a_g}^{(l)}$ is a Boolean vector defined according to the direction of the seismic acceleration $a_g(t)$. Then, Principal Component Analysis (PCA) was applied to a dataset $\mathbf{X}$ corresponding to the deformational component of the PS calculated in with Eq. (3),

$$\mathbf{X} = \begin{bmatrix} \widetilde{\mathbf{u}}_1^{P,r} & \dots & \widetilde{\mathbf{u}}_n^{P,r} \end{bmatrix} \tag{8}$$

The key idea of PCA is to provide a separated representation of a number of correlated variables considering a smaller number of uncorrelated variables while preserving the overall process variance. An orthogonal transformation to the basis of the eigenvectors of the sample covariance matrix is performed, and the data are projected onto the subspace spanned by the eigenvectors corresponding to eigenvalues sorted in descending order, [15]. This transformation decorrelates the signal components and maximizes the preserved variance. In detail, for any real (*m* x *n*) matrix $\mathbf{X}$ there exists a real factorization called Singular Value Decomposition (SVD) that can be written as,

$$\mathbf{X} = \mathbf{U}\boldsymbol{\Sigma}\mathbf{V}^T \tag{9}$$

where $\mathbf{U}$ is an (*m* x *m*) orthonormal matrix whose columns $\mathbf{u}_i$, namely the left singular vectors, represents the Proper Orthogonal Modes (POMs) while $\mathbf{V}$ is an (*n x n*) orthonormal matrix, whose column vectors $\mathbf{v}_i$, namely the right singular vectors, represent the time modulation of the corresponding POMs. $\boldsymbol{\Sigma}$ is an (*m x n*) pseudo-diagonal and semi-positive definite matrix with singular values σ_i as diagonal entries. Singular values relate to the eigenvalues of the autocovariance matrix of the process $\mathbf{X}$ as,

$$\{\sigma_1^2 \quad \dots \quad \sigma_m^2\} = eig\big((\mathbf{X} - \boldsymbol{\mu}_\mathbf{X})(\mathbf{X} - \boldsymbol{\mu}_\mathbf{X})^T\big) \tag{10}$$

where $\boldsymbol{\mu}_\mathbf{X}$ is a matrix of repeated vectors of time averaged values of $\mathbf{X}$. Since gravity (constant) loads are excluded, $\boldsymbol{\mu}_\mathbf{X}$ is almost null and thus very small compared to $\mathbf{X}$. Accordingly, the original data set $\mathbf{X}$ can be reconstructed up to the desired degree of approximation by retaining a reduced number $q < m$ of POM,

$$\big(\widetilde{\mathbf{X}} - \boldsymbol{\mu}_\mathbf{X}\big) = \sum_{i=1}^{q} \sigma_i \mathbf{u}_i \mathbf{v}_i^T \tag{11}$$

The energy fraction carried by the i-th POM is defined as $E_i = \sigma_i^2/E$ is, considering a total data energy $E = \sum_{i=1}^{m} \sigma_i^2$. Figure 7 reports the energy fraction of the first ten POMs.

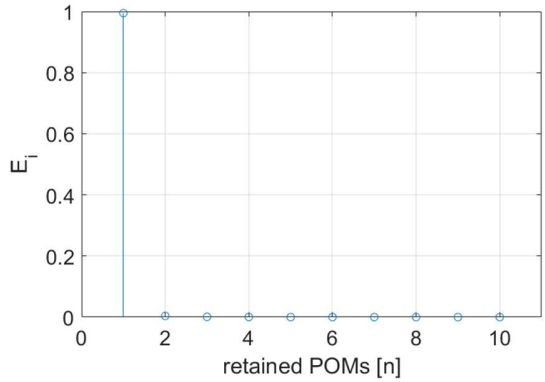

Figure 7: Distribution of POM energy.

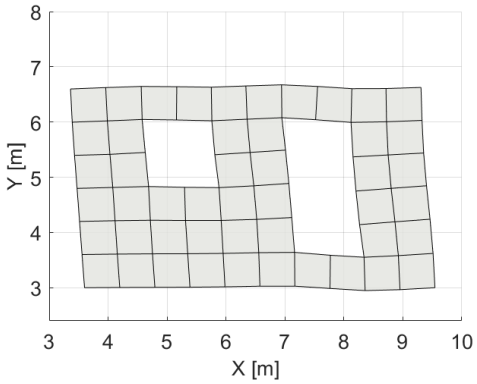

Figure 8: POM #1 deformed shape.

As can be appreciated from Figure 7, the almost total energy of the deformational component of the displacement response of the PS is carried by the first POM, which is depicted in Figure 8.

4 VALIDATION OF THE SUBSTRUCTURING METHOD

In order to impose piecewise affine displacement fields along subdomain boundaries and reduce the number of connected nodes, rigid ISs are applied on both NS and PS boundaries. Figure 9 depicts the Modified (M)-FE partitioned model of the PMFS including ISs, which was used to validate the presented substructuring method.

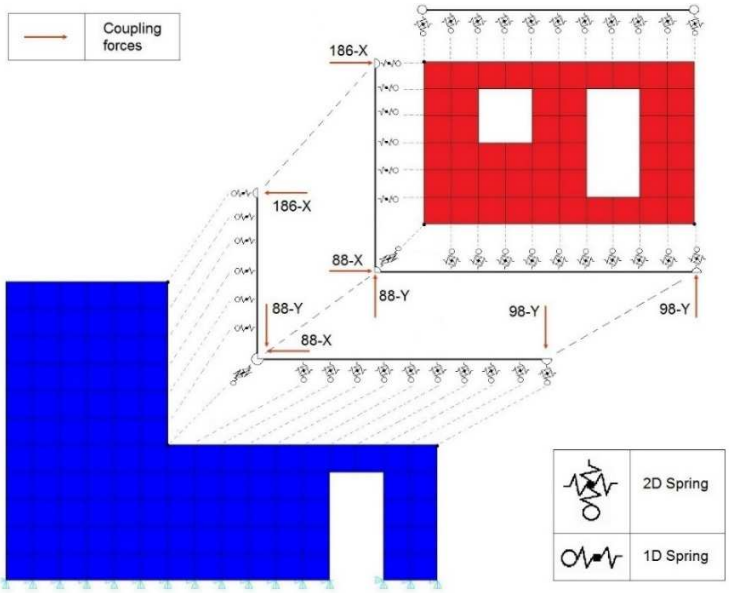

Figure 9: M-FE partitioned model of the PMFS

As can be appreciated from Figure 9, both ISs are based on rigid spring and beam elements, which enforce affine displacement fields along PS and NS boundaries. In detail, simplified coupling conditions neglect continuity of vertical and horizontal shear along the vertical and horizontal edges of the PS interface, respectively. As a result, the number of coupled DOFs is reduced to 4. The system of coupled equations of motion of the M-FE partitioned model read,

$$\begin{cases} \mathbf{M}^{N,I}\ddot{\mathbf{u}}^{N,I} + \mathbf{C}^{N,I}\dot{\mathbf{u}}^{N,I} + \mathbf{K}^{N,I}\mathbf{u}^{N,I} = \mathbf{L}^{N,I^T}\boldsymbol{\Lambda}^{N,I} + \mathbf{F}^{N,I}(t) \\ \mathbf{M}^{N}\ddot{\mathbf{u}}^{N} + \mathbf{C}^{N}\dot{\mathbf{u}}^{N} + \mathbf{K}^{N}\mathbf{u}^{N} = \mathbf{L}^{N^T}\boldsymbol{\Lambda}^{N} + \mathbf{F}^{N}(t) \\ \mathbf{M}^{P,I}\ddot{\mathbf{u}}^{P,I} + \mathbf{C}^{P,I}\dot{\mathbf{u}}^{P,I} + \mathbf{K}^{P,I}\mathbf{u}^{P,I} = \mathbf{L}^{P,I^T}\boldsymbol{\Lambda}^{P,I} + \mathbf{F}^{P,I}(t) \\ \mathbf{M}^{P}\ddot{\mathbf{u}}^{P} + \mathbf{C}^{P}\dot{\mathbf{u}}^{P} + \mathbf{K}^{P}\mathbf{u}^{P} = \mathbf{L}^{P^T}\boldsymbol{\Lambda}^{P} + \mathbf{F}^{P}(t) \end{cases} \tag{12a}$$

$$\begin{cases} \mathbf{L}^{N,I}\dot{\mathbf{u}}^{N,I} + \bar{\mathbf{L}}^{N,I}\dot{\mathbf{u}}_g = \mathbf{0} \\ \mathbf{L}^{N}\dot{\mathbf{u}}^{N} + \bar{\mathbf{L}}^{N}\dot{\mathbf{u}}_g = \mathbf{0} \\ \mathbf{L}^{P,I}\dot{\mathbf{u}}^{P,I} + \bar{\mathbf{L}}^{P,I}\dot{\mathbf{u}}_g = \mathbf{0} \\ \mathbf{L}^{P}\dot{\mathbf{u}}^{P,D} + \bar{\mathbf{L}}^{P}\dot{\mathbf{u}}_g = \mathbf{0} \end{cases} \tag{12b}$$

$$\bar{\mathbf{L}}^{N,I^T}\boldsymbol{\Lambda}^{N,I} + \bar{\mathbf{L}}^{N^T}\boldsymbol{\Lambda}^{N} + \bar{\mathbf{L}}^{P,I^T}\boldsymbol{\Lambda}^{P,I} + \bar{\mathbf{L}}^{P^T}\boldsymbol{\Lambda}^{P} = \mathbf{0} \tag{12c}$$

where subscripts N,I and P,I refer to numerical and physical ISs, respectively. The static response of the modified partitioned model was calculated with a version of the FR algorithm, [13], enhanced to LLM framework. The following time history restart analysis was calculated with a version of [14], enhanced to LLM framework, [12]. Figure 10 compares the displacement response of DOF 196-X and DOF 196-Y obtained from the R-FE and M-FE partitioned models.

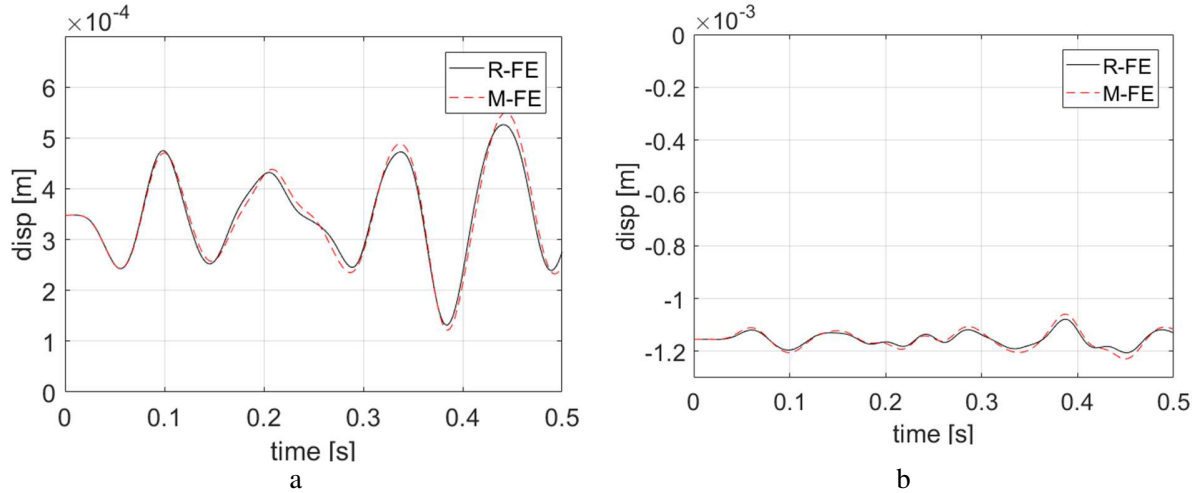

a b

Figure 10: Displacement response of for M-FE partitioned model: a) DOF 196-X; and b) DOF 196-Y

As can be appreciated from Figure 10, the M-FE partitioned model accurately reproduces both horizontal and vertical displacement responses of the R-FE partitioned model. Figure 11 depicts a possible experimental setup for the PS.

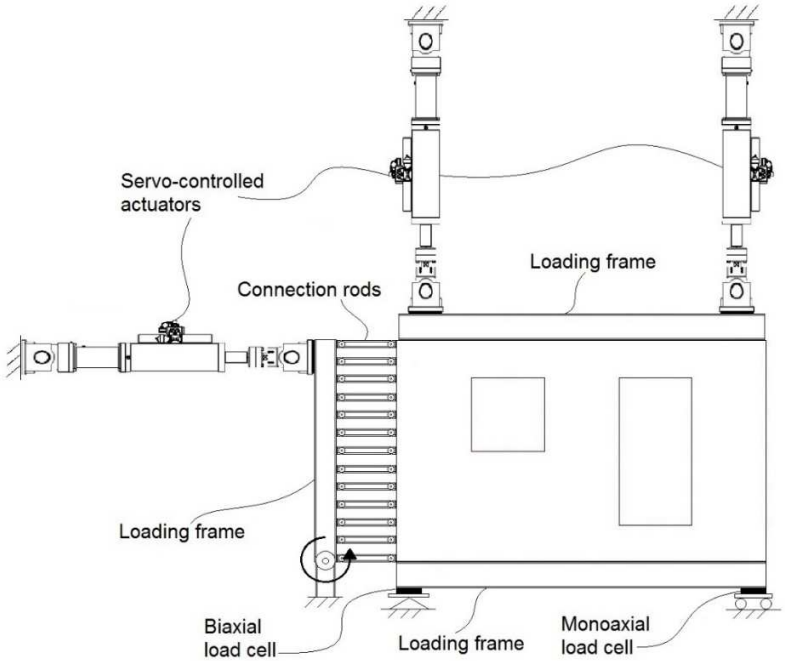

Figure 11: Experimental setup

As shown in Figure 11, rigid frames, anchors and connecting rods form the physical IS and impose an affine interface displacement field to the PS, which is tested in statically determined configuration. Load cells installed on actuators and supports measure restoring force feedbacks.

5 CONCLUSIONS

This paper presented a new substructuring method for performing hybrid simulation of planar masonry structures, which are characterized by distributed physical and numerical subdomain boundaries. Rigid interface super-elements are introduced to impose affine displacement fields at subdomain boundaries with a reduced number of connection degrees-of-freedom, which allows for reducing the number of actuators of the relevant experimental setup. In detail, rigid beam and link elements forms the NS interface super-element while steel frames, anchors and connection rods form the PS interface super-element. The numerical validation of this procedure is illustrated for a planar masonry facade system, which is virtually substructured using a typical three-actuator test setup for quasi-static cyclic testing of masonry wall specimens.

REFERENCES

[1] Takanashi, K., Udagawa, K., Seki, M., Okada, T. and Tanaka, H. (1975). "Non-linear earthquake response analysis of structures by a computer-actuator on-line system." *Bulletin of*

Earthquake Resistant Structure Research Center, Institute of Industrial Science, University of Tokyo, Tokyo.

[2] Stojadinovic, B., Mosqueda, G. and Mahin S.A. (2006). "Event-Driven Control System for Geographically Distributed Hybrid Simulation." *ASCE Journal of Structural Engineering*, 132(1), 68-77.

[3] Paquette, J. and Bruneau, M. (2003). "Pseudo-Dynamic Testing of Unreinforced Masonry Building with Flexible Diaphragm." *M. ASCE2*, DOI: 10.1061/~ASCE!0733-9445~2003!129:6~708!.

[4] Paquette, J., Bruneau, M. (2006). "Pseudo-dynamic testing of unreinforced masonry building with flexible diaphragm and comparison with existing procedures." *Construction and Building Materials*, 20, 220-228.

[5] Pinto, A., Molina, J., Pegon, P., Renda, V. (2001). "Protection of the cultural heritage at the ELSA Laboratory." *ELSA*, IPSC, Joint Research Centre, European Commission, I-21020 Ispra (VA), Italy.

[6] Buonopane, S.G. and White, R.N. (1999). "Pseudodynamic testing of masonry infilled reinforced concrete frame." *J. Struct. Eng.*, ASCE 125, 578-589.

[7] Mosalam, K.M., White, R.N. and Ayala, G. (1998). "Response of infilled frames using pseudo-dynamic experimentation." *Earthquake Engineering and Structural Dynamics*, 27, 589-608.

[8] Hashemi, M.J., and Mosqueda, G. (2014). "Innovative substructuring technique for hybrid simulation of multistory buildings through collapse." *Earthquake Engineering and Structural Dynamics*, doi:10.1002/eqe.2427.

[9] Bakhaty, A.A., Govindjee, S., and Mosalam, K.M. (2016). "Theoretical Evaluation of Hybrid Simulation Applied to Continuous Plate Structures." *Journal of Engineering Mechanics*, 142(12).

[10] MATLAB and Statistics Toolbox Release R2016b, The MathWorks, Inc., Natick, Massachusetts, United States.

[11] ANSYS, ANSYS Academic Research, Release 16.2, 2016.

[12] Park K.C., Felippa C.A., Gumaste U.A. (2000). "A localized version of the method of Lagrange multipliers and its applications." *Computational Mechanics*, 24, 476-490.

[13] Farhat, C. and Roux, F.-X. (1991). "A method of finite element tearing and interconnecting and its parallel solution algorithm." *Int J Num Meth Engng*, 32, 1205-1227, doi: 10.1002/nme.1620320604.

[14] Gravouil, A., Combescure, A. (2001). "Multi-time-step explicit – implicit method for non-linear structural dynamics." *International Journal for Numerical Methods in Engineering*, 199-225.

[15] Kerschen, G., Golinval, J., Vakakis, A.F. and Bergman L. (2005). "The Method of Proper Orthogonal Decomposition for Dynamical Characterization and Order Reduction of Mechanical Systems: An Overview." *Nonlinear Dynamics*, 41(1-3), 147–169, doi:10.1007/s11071-005-2803-2.